R_2^* Mapping for Robust Brain Function Detection in the Presence of Magnetic Field Inhomogeneity

Giang Chau Ngo[1], *Student Member, IEEE*, and Bradley P. Sutton[1], *Member, IEEE,*

***Abstract*— T_2^* mapping or R_2^* mapping for brain function offers advantages such as providing quantitative measurements independent of the MRI acquisition parameters (e.g. echo time TE). However, magnetic field susceptibility in the human brain can prevent an accurate estimation of R_2^*, which in turn impacts the ability to study brain function. The present work investigates the effects of in-plane magnetic susceptibility-induced magnetic field gradients on R_2^* decay. An iterative method is developed for R_2^* estimation with an increased robustness to field inhomogeneity. The new method is further tested in a visual fMRI experiment with and without magnetic field gradients and its performance is compared to a standard BOLD fMRI and a BOLD fMRI based on echo summation. Reduced sensitivity in fMRI to in-plane magnetic gradients is obtained with the present methodology.**

I. Introduction

Since its discovery in the 1990's [1], the blood oxygen level dependent (BOLD) contrast has been extensively used in functional magnetic resonance imaging (fMRI) studies. BOLD contrast in T_2^*-weighted images is dependent on the acquisition parameters such as the echo time, TE, and varies through the brain. Therefore, several studies have attempted to provide quantitative measurements of brain function by looking directly at the transverse spin relaxation parameter, T_2^*, or its inverse, R_2^* [2], [3], [4]. In addition, artifacts such as inflow effects, which are not related to brain function, only appear on the intensity images I_0 (echo time of 0 s), and thus are not captured in R_2^* maps [5]. In most studies, R_2^* maps are obtained by acquiring T_2^*-weighted images at different echo times with multi-echo time sequences, and fitting the parameters of the exponential signal decay.

However, magnetic susceptibility differences due to air/tissue interfaces in the human brain create macroscopic magnetic field gradients that disrupt the uniformity of the magnetic field. They result in image distortions, signal loss and k-space distortions. Although many strategies have been developed to minimize susceptibility effects [6], [7], BOLD sensitivity variations in fMRI due to magnetic field inhomogeneity have not been completely addressed. Deichmann *et al.* [8] showed that magnetic susceptibility resulted in a shift in the echo time, causing changes in the acquired BOLD signal without any major impact on the overall image structure, quality and intensity.

∗The project described was supported by Award Number R21EB010095 from NIBIB. The content is solely the responsibility of the authors and does not necessarily reflect the views of the NIBIB or NIH.

[1]The authors are with the Department of Bioengineering at the University of Illinois at Urbana-Champaign and the Beckman Institute, University of Illinois at Urbana-Champaign, Urbana IL, United States. gngo at illinois.edu, bsutton at illinois.edu

Other works have indicated that magnetic field inhomogeneity has also a direct impact on the R_2^* exponential decay [9], [10]. Fernanez-Seara *et al.* [9] showed that through-plane magnetic gradients created a sinc modulation of the exponential decay which needed to be considered when estimating R_2^*. Another study from Yang *et al.* [10] modeled a quadratic term in the exponential decay due to magnetic inhomogeneity at high magnetic field. Other studies focused on acquisition methods to alleviate the impact of magnetic gradients [11], [12]. However, these methods tend to lengthen already long acquisition times and may not be suited for fMRI when a short acquisition time is needed.

So far, most techniques have tackled signal loss caused by susceptibility-induced through-plane gradients and few previous works have looked into the impact of in-plane magnetic field gradients [12], [13], [14]. For example, in addition to a z-shimming technique to compensate for through-plane magnetic gradient, Bauderexel *et al.* [12] discarded data points where in-plane magnetic gradients induced important signal loss to provide a more accurate estimation of R_2^*. Moreover, some other studies developed iterative methods to jointly estimate the field map, the decay rate map and the intensity images I_0 [13], [14]. A joint estimation can handle the R_2^* decay as well as any magnetic drift in the field map which can occur during the acquisition readout. Olfasson *et al.* [14] applied this method for brain function detection during a motor task. Their iterative method was able to detect more active voxels than a standard BOLD fMRI and a R_2^* fMRI based on an exponential fit. However, the impact of magnetic field gradients was not considered in their study. Despite these important steps forward, it still remains a challenge to obtain accurate estimations of R_2^* maps for functional imaging in the presence of in-plane susceptibility-induced magnetic field gradients.

In this paper, the impacts of susceptibility induced in-plane magnetic gradients on R_2^* decay are further investigated through the development and validation of a signal model. For this purpose, the signal model described in [15], [16] was extended to include the R_2^* signal decay [17] but also any intra-voxel magnetic field gradients. An iterative method is applied to estimate R_2^*, as well as the field map and the I_0 images. Further, an efficient multi-echo acquisition is proposed that takes advantage of parallel imaging and is used for investigating the effect of magnetic inhomogeneity on brain function detection. A visual fMRI experiment using the multi-echo sequence is performed and used to obtain a standard BOLD signal, a BOLD signal based on echo summation and a time series of R_2^* maps. The performance of

978-1-4244-7929-0/14/$26.00 ©2014 IEEE

the three methods for brain function detection are compared.

II. Theory

A. Signal model

In MRI, the measured signal can be written in a discrete form, ignoring the T_1 relaxation [15], [16]:

$$s(t) \approx \sum_{n=0}^{N} \phi(r_n) f_n \mathrm{e}^{-(iw_n + G_n(x,y) + R^*_{2,n})t} \mathrm{e}^{-i2\pi(k(t).r_n)} \quad (1)$$

$$G_n(x,y) = X_n(x - x_n) + Y_n(y - y_n) \quad (2)$$

Where ϕ is the voxel indicator basis function at the location r_n, f_n is the object to be imaged, w_n and $R^*_{2,n}$ are the field map and R^*_2 value, and X_n and Y_n are the magnetic field gradients in the x- and y-directions. Intra-voxel in-plane magnetic field gradients are taken into account through the term X_n and Y_n. In this paper, the through-plane magnetic gradients are not taken into account in the current model. A unidirectional in-plane gradient is applied in the phantom study, and the through-plane magnetic gradients are reduced in the human study by using thinner slices. These settings minimize the effects of through-plane magnetic gradients in both experiments. These gradients will be included in future work by adding a $Z_n(z - z_n)$ term in the G_n expression.

Equation 1 can be rewritten in a matrix-vector form:

$$y = A(w, R^*_2) f + \varepsilon \quad (3)$$

where y is the measured signal, ε corresponds to the noise, f is the vector of f_n, and the components of the matrix $A(w, R^*_2)$ are defined as:

$$a_{m,n} = \phi(r_n) \mathrm{e}^{-(iw_n + G_n(x_m, y_m) + R^*_{2,n})t_m} \mathrm{e}^{-i2\pi(k(t_m).r_n)} \quad (4)$$

B. Nonlinear least squares joint estimation

Equation 3 allows us to estimate f, w and R^*_2 using an iterative algorithm. The objective function to minimize is defined as follows:

$$\psi = \frac{1}{2} \| y - A(w, R^*_2) f \|^2 + \beta_1 R(f) + \beta_2 R(w) + \beta_3 R(R^*_2) \quad (5)$$

$R(f)$, $R(w)$ and $R(R^*_2)$ are regularization penalty functions that penalize spatial derivatives of the image, the field map and the R^*_2 map respectively. The β_i coefficients are constants used to control the regularization penalty of each component [16], [17]. This minimization problem is solved by using a nonlinear conjugate gradient method similar to [18]. Fast computation is achieved by using the NUFFT (Nonuniform Fast Fourier Transforms) and time segmentation [15], [16].

III. Methods

The impact of in-plane magnetic field gradients on the T^*_2 decay was first studied on a phantom and later on a human subject. The signal model was validated by correlating the acquired signal decay to simulated data. A visual fMRI experiment was performed to assess the robustness of the proposed estimation method for brain function detection.

A. Study of the R^*_2 decay in the presence of in-plane magnetic gradients

Data on a phantom were acquired on a 3T Trio (Siemens) with a 12-channel head coil. A multi-echo, single-shot, spiral-out sequence was used with the following parameters: 64x64 matrix; 24cm FOV; 3.75x3.75x4mm voxel size; 2s TR, eighteen TE values from 10ms and 130ms. A purposeful mis-shim on the y-gradient channel creating magnetic gradients of 20Hz/cm through the object was also applied. This shim condition is referred as a bad shim. The case of no magnetic gradients is called a good shim. Images were acquired in both shim conditions and reconstructed with a standard gridding method. Simulated data were also generated using the present model and an acquired field map. The R^*_2 value of the phantom was found to be $15s^{-1}$ in the good shim. This value of R^*_2 was used for the simulation.

Axial brain scans were also acquired with the same sequence and the following parameters: 10 axial slices 2mm thick; fourteen TEs from 15ms to 140ms; 3s TR. A 20Hz/cm in-plane magnetic gradients, well within the range of magnetic susceptibility gradient at 3T, was also applied in the y-direction. The images were reconstructed with 1) a standard gridding method and 2) gridding with conjugate phase method (field correction, FC).

B. Impact of susceptibility-induced magnetic field gradient on brain function detection

A visual fMRI experiment was performed on a single subject using a spiral-out single shot multi-echo sequence. Since the visual cortex does not have strong field inhomogeneity, this region of the human brain was suitable for assessing the impact of field gradients under a good shim and a bad shim condition. In order to shorten the acquisition time, parallel imaging with a reduction factor of 2 was used with a 12 channel head coil. The following parameters were used: 10 coronal slices; 64x64 matrix; 24cm FOV; 3.75x3.75x2mm voxel size; 1.5s TR; four TE values (20/40/60/80ms). A visual task composed of 21 off/on periods of 30s each is used in two conditions: with a good shim and a bad shim (z-gradient of 15-20Hz/cm). The slices were slightly tilted to avoid aliasing with the subject's shoulder. Four slices were used for studying the brain function.

For comparison, T^*_2-weighted images from one of the echoes (TE=40ms) were reconstructed using a SENSE reconstruction and used as standard BOLD images. The time series was analyzed with FSL to define the activated areas corresponding to the visual task. A clustering constraint with a z-score threshold of 4 and a p-value of 0.01 were used to obtain the z-score maps. The T^*_2-weighted images from the four echoes were also averaged. The resulting time series was analyzed with the same parameters as the standard BOLD fMRI and was called the average BOLD signal.

For each multi-echo acquisition, a R^*_2 map was estimated by using the joint estimation algorithm, resulting in a time series of R^*_2 maps. For the estimation of the first R^*_2 map in the time series, a field map acquired at the beginning of the scan session and an image reconstructed from the first

echo were used as initial values for w and f respectively. The initial R_2^* map was set to zero. To estimate the next R_2^* maps in the time series, the initial R_2^* map and the I_0 image were defined as the one estimated at the first multi-echo acquisition, whereas the initial field map was the one estimated at the previous multi-echo acquisition. Thus, the field map was serially initialized. This method allowed us to reduce the number of iterations needed, while tracking any drifts in the magnetic field. An analysis similar to the BOLD fMRI was performed with FSL on the time series of R_2^* maps to determine the activated regions related to the visual task.

Activations were compared between good shim and bad shim conditions, as well as between standard BOLD fMRI, average BOLD fMRI and fMRI based on R_2^* maps. The number of activated voxels in each slice were compared. A z-score threshold of 5 was used to define the activated voxels. This value was chosen to avoid taking into account the voxels considered activated in the skull. In order to compare these values, the number of voxels related to the brain were estimated for each slice, and a percentage of the activated voxels per slice were calculated.

Moreover, pixel by pixel percentage of error of the z-score maps were also calculated by considering the good shim maps as the true maps. Pixels that were not considered as activated in the good shim but activated in the bad shim were discarded and the converse.

IV. Results and Discussion

A. Magnetic susceptibility induced in-plane magnetic gradients on R_2^* decay

Fig. 1 shows the MRI signal evolution on a phantom at different TEs, in the case of a 20Hz/cm magnetic gradient across the object. In the presence of in-plane magnetic susceptibility-induced gradients, the R_2^* signal decay does not behave as an exponential function and the behavior varies across the image. The deviations from the exponential decay are mainly due to distortions in the k-space trajectory. Magnetic susceptibility leads to variable sampling densities in the spiral trajectory and distorts the point spread function (psf). In addition, the echo times are shifted due to field inhomogeneitiy and the center of k-space is not sampled, resulting in signal losses at high TE values. In Fig. 1, the signal is also compared to data simulated using the model described in the theory section. By taking into account the intra-voxel magnetic gradients, we can accurately predict the behavior observed on the acquired data.

Moreover, gridding or field correction methods are not able to correct the signal decay and the image distortions in the presence of magnetic field gradients. Fig. 2 shows an axial image of the brain reconstructed with two different approaches: a gridding method (straight lines) and a field correction (dashed line). The signal intensity of different ROIs for the different reconstruction strategies are plotted against TEs. Even though the image is less distorted with the field correction method, the R_2^* signal evolution still deviates from an exponential decay. Indeed, intra-voxel magnetic gradients are not corrected with this method. These results

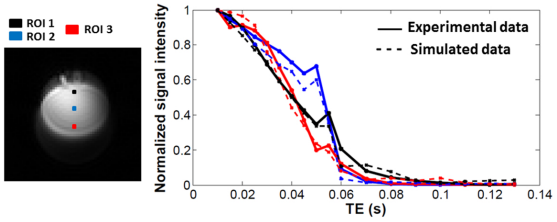

Fig. 1. T_2^* weighted images of a phantom at TE=10ms and signal evolutions of multi-echo gradient echo acquisition under a 20 Hz/cm gradient in the y-direction (vertical axis on the image). Straight lines are experimental signals and dotted lines are from simulation.

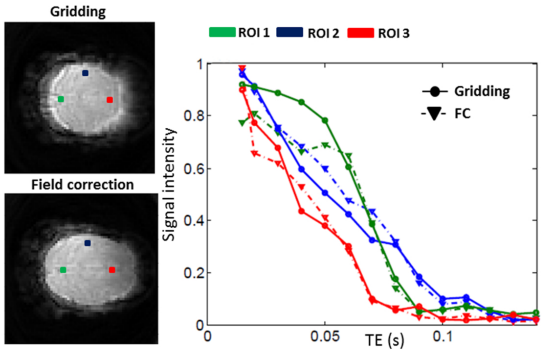

Fig. 2. Axial human brain slice under a 20Hz/cm gradient in the y-direction (horizontal axis on the images) at TE=20ms reconstructed with a gridding and a field correction methods. Signal evolutions for the different ROIs and for the different reconstruction strategies.

show that estimating R_2^* by an exponential fit may lead to incorrect values. In order to accurately estimate R_2^* in the presence of high magnetic field inhomogeneity, it is necessary to use an iterative method.

B. Brain function detection in the presence of in-plane magnetic susceptibility

It has been shown that an increase of TE leads to an increase of the BOLD contrast [8]. In the bad shim case, since a spiral out sequence is used, the achieved echo times are longer than intended, resulting in a higher BOLD contrast. Therefore some areas of the brain demonstrate artifactually higher activations during the task.

Fig. 3 shows z-score maps, for one slice, for a standard BOLD technique in the case of a good shim (GS) (a) and a bad shim (BS) (b), for the average BOLD (BOLD Mean) in the good shim (d) and the bad shim (e) case, as well as for the R_2^*-based fMRI in the case of a good shim (g) and a bad shim (h). Table I summarizes the number of voxels activated in each slice and their corresponding percentage. The number of voxels in the visual cortex in slice 1 is approximately 477, 442 in slice 2, 398 in slice 3 and 334 in slice 4. The standard BOLD fMRI and the average BOLD fMRI methods have discrepancies in the coverage of the activation areas between the case of a good shim and a bad shim. Broader activation is detected in the bad shim case (Table I). Conversely, with the R_2^*-based technique, the areas corresponding to the visual task are very similar. In addition, Fig. 3 also shows the percentage of error in the z-score maps for the standard

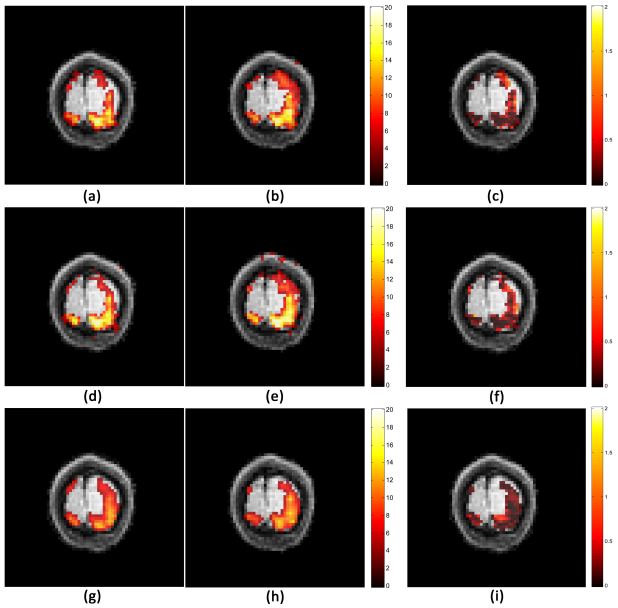

Fig. 3. Activation map for (a) BOLD good shim (b) BOLD bad shim (d) Average BOLD good shim (e) Average BOLD bad shim (g) R_2^* fMRI good shim (h) R_2^* fMRI bad shim. Percentage of error in the z-score are shown for (c) the standard BOLD, (f) the average BOLD and (i) the R_2^* fMRI. Pixels showing activation in the good shim case but not in the bad shim and the converse, were discarded.

TABLE I

NUMBER AND PERCENTAGE (IN PARENTHESIS) OF VOXELS ACTIVATED IN THE 4 DIFFERENT SLICES

	Slice 1	**Slice 2**	**Slice 3**	**Slice 4**
BOLD GS	163 (34.2)	143 (32.4)	111 (27.9)	92 (27.5)
BOLD BS	188 (39.4)	167 (37.8)	140 (35.2)	109 (32.6)
BOLD Mean GS	185 (38.8)	147 (33.2)	114 (28.6)	90 (26.9)
BOLD Mean BS	201 (42.1)	177 (40.0)	142 (35.7)	100 (29.9)
R_2^* GS	163 (34.2)	137 (31.0)	121 (30.4)	93 (27.8)
R_2^* BS	160 (33.5)	146 (33.0)	115 (28.9)	95 (28.4)

BOLD (c), the average BOLD (f) and the R_2^* based fMRI (i). The proposed method shows overall smaller percentage of error (BOLD: $29.9 \pm 27\%$; BOLD mean: $29.3 \pm 27\%$; R_2^*: $21.1 \pm 19\%$) and more consistent error across slice than the two other methods.

These results suggest that our method is robust to the effects of magnetic field gradients. In addition, the R_2^* mapping for fMRI has potential to detect more active voxels than a standard BOLD, which has been observed in [14].

V. CONCLUSION

The present study showed that in-plane magnetic field susceptibility has a strong impact on R_2^* decay, which can lead to inaccurate R_2^* estimations. Unlike through-plane magnetic gradients, the impact of in-plane magnetic gradients cannot be easily modeled as an additional function [9], [10]. An iterative method based on a signal model for R_2^* decay was proposed and proved to be robust to the magnetic field inhomogeneity. The proposed method showed reduced differences between good shim and bad shim in activation areas, as well as lower errors in z-score maps, compared to a standard BOLD and an average BOLD technique. Current work is being conducted to further extend these results by including more subjects in the study. Even though this paper focuses on brain function, these findings can impact any work based on gradient echo imaging or T_2^* estimation.

ACKNOWLEDGMENTS

We thank the Nadine Barrie Smith Memorial Fund for their support.

REFERENCES

[1] S. Ogawa, T.-M. Lee, A. Nayak, and P. Glynn, "Oxygenation-sensitive contrast in magnetic resonance image of rodent brain at high magnetic fields," *Magn. Res. Med.*, vol. 14, no. 1, pp. 68–78, 1990.

[2] A. B. A. Wennerberg, T. Jonsson, H. Forssberg, and T.-Q. Li, "A comparative fmri study: T2*-weighted imaging versus r2*-mapping," *NMR in Biomedicine*, vol. 14, no. 1, pp. 41–47, 2001.

[3] G. Hagberg, I. Indovina, J. Sanes, and S. Posse, "Real-time quantification of t2* changes using multiecho planar imaging and numerical methods," *Magn. Res. Med.*, vol. 48, no. 5, pp. 877–882, 2002.

[4] M. Barth, A. Metzler, M. Klarhfer, S. Rll, E. Moser, and D. Leibfritz, "Functional mri of the human motor cortex using single-shot, multiple gradient-echo spiral imaging," *Magn. Res. Imag.*, vol. 17, no. 9, pp. 1239–1243, 1999.

[5] O. Speck and J. Hennig, "Functional imaging by i0- and t2*-parameter mapping using multi- image epi," *Magn. Res. Med.*, vol. 40, no. 2, pp. 243–248, 1998.

[6] P. Jezzard and R. Balaban, "Correction for geometric distortion in echo planar images from b0 field variations," *Magn. Res. Med.*, vol. 34, no. 1, pp. 65–73, 1995.

[7] J. Wilson and P. Jezzard, "Utilization of an intra-oral diamagnetic passive shim in functional mri of the inferior frontal cortex," *Magn. Res. Med.*, vol. 50, no. 5, pp. 1089–1094, 2003.

[8] R. Deichmann, O. Josephs, C. Hutton, D. Corfield, and R. Turner, "Compensation of susceptibility-induced bold sensitivity losses in echo-planar fmri imaging," *NeuroImage*, vol. 15, no. 1, pp. 120–135, 2002.

[9] M. Fernndez-Seara and F. Wehrli, "Postprocessing technique to correct for background gradients in image-based r2* measurements," *Magn. Res. Med.*, vol. 44, no. 3, pp. 358–366, 2000.

[10] X. Yang, S. Sammet, P. Schmalbrock, and M. Knopp, "Postprocessing correction for distortions in t2* decay caused by quadratic cross-slice b0 inhomogeneity," *Magn. Res. Med.*, vol. 63, no. 5, pp. 1258–1268, 2010.

[11] S. Posse, Z. Shen, V. Kiselev, and L. Kemna, "Single-shot t2* mapping with 3d compensation of local susceptibility gradients in multiple regions," *NeuroImage*, vol. 18, no. 2, pp. 390–400, 2003.

[12] S. Baudrexel, S. Volz, C. Preibisch, J. Klein, H. Steinmetz, R. Hilker, and R. Deichmann, "Rapid single-scan t2*-mapping using exponential excitation pulses and image-based correction for linear background gradients," *Magn. Res. Med.*, vol. 62, no. 1, pp. 263–268, 2009.

[13] T. Knopp, H. Eggers, H. Dahnke, J. Prestin, and J. Sngas, "Iterative off-resonance and signal decay estimation and correction for multi-echo mri," *IEEE Trans. Med. Imag.*, vol. 28, no. 3, pp. 394–404, 2009.

[14] V. Olafsson, D. Noll, and J. Fessler, "Fast joint reconstruction of dynamic r2* and field maps in functional mri," *Magn. Res. Med.*, vol. 27, no. 9, pp. 1177–1188, 2008, cited By (since 1996)11.

[15] B. Sutton, D. Noll, and J. Fessler, "Fast, iterative image reconstruction for mri in the presence of field inhomogeneities," *IEEE Trans. Med. Imag.*, vol. 22, no. 2, pp. 178–188, 2003.

[16] B. Sutton, D. Noll, and J. Fessler, "Dynamic field map estimation using a spiral-in/spiral-out acquisition," *Magn. Res. Med.*, vol. 51, no. 6, pp. 1194–1204, 2004.

[17] B. Sutton, S. Peltier, J. Fessler, and D. Noll, "Simultaneous estimation of i0, r2* and field map using a multi echo-spiral acquisition," in *Proc. Int. Soc. Mag. Res. Med.*, 2002, p. 1323.

[18] M. Lustig, D. Donoho, and J. Pauly, "Sparse mri: The application of compressed sensing for rapid mr imaging," *Magn. Res. Med.*, vol. 58, no. 6, pp. 1182–1195, 2007.